2009 American Control Conference
Hyatt Regency Riverfront, St. Louis, MO, USA
June 10-12, 2009

Active Power Filter for Three-Phase Current Harmonic Cancellation and Reactive Power Compensation

Siyu Leng, Wenxin Liu, II-Yop Chung and David Cartes

Abstract – **To address power quality problems in industrial power systems, a new control scheme for three-phase active power filter is proposed. The control scheme includes two functional modules such as a current harmonic cancellation module and a reactive power compensation module. The current harmonic cancellation module is based on a multiple adaptive feed-forward cancellation algorithm for selective current harmonic identification. The reactive power compensation module utilizes the measured voltage and the estimated fundamental current to calculate reactive power. After the above information has been calculated, the corrective current reference signals can be generated for the active filter. In this way, the two control functions are integrated together so that one active filter can accomplish two functions simultaneously. Simulation results under different operating conditions demonstrate that the proposed control scheme can successfully cancel harmonic current and compensate reactive power at the point of common coupling.**

I. Introduction

MODERN power industries are using more and more semiconductor-based devices, such as adjustable speed drives，furnaces, computer power supplies, uninterruptible power supplies, etc. Even though these devices are economical, flexible and energy efficient, they may degrade power quality by creating harmonic currents and consuming excessive reactive power. The above phenomena can cause many problems such as resonance, excessive neutral currents, low power factor and so on. It may even cause malfunctions in control, communication and automation systems. Thus, the associated power quality problems have to be addressed.

Traditionally, passive shunt filters are installed near nonlinear loads to mitigate harmonic currents. However, the passive filters have drawbacks such as fixed compensation, large size, and resonance. These limitations can be overcome by power electronics solution – active power filters. Compared with conventional passive filters, modern active power filters are superior in filtering performance, smaller in physical size and more flexible in application [1]. The typical configuration of a voltage source active power filter is shown in Fig. 1. The active power filter detects harmonic information in non-linear load currents and actively injects counter harmonic currents to the grid so that the currents at Point of Common Coupling (PCC) approximate sinusoidal waveforms.

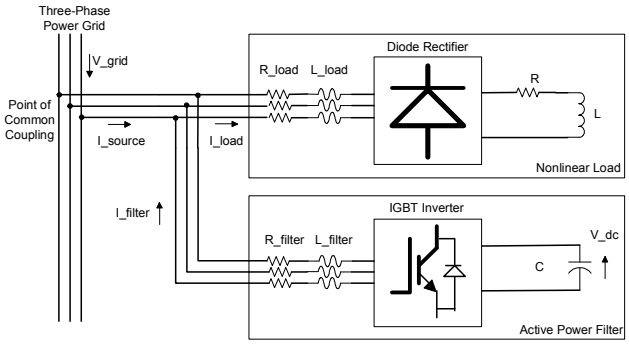

Fig. 1. Voltage source active power filter configuration

Many harmonic detection techniques for active power filters have been studied. In frequency domain, Discrete Fourier Transform (DFT) and Fast Fourier Transform (FFT) have been widely used [2-3]. The main disadvantage of these techniques is the time delay associated with sampling and computation of Fourier coefficients, which makes them difficult for real-time application on dynamically varying load.

In the time domain, a number of methods have been proposed. Notch filters or band pass filters [4-5] were used to extract harmonics but it was difficult to implement the ideal amplitude and phase characteristics of the filters and its performance is also sensitive to power system parameter variation. A popular method for harmonic detection is based on p-q theory via Clarke transformation [6-7]. This technique uses both current and voltage information to compute the harmonic compensating signals. However, if the input voltage contains harmonics, the resulting performance has been proven to be poor [8].

Another popular method is the synchronous rotating d-q reference frame methods [9-11]. This algorithm relies on the

Manuscript received September 22, 2008.

The authors are with Center for Advanced Power Systems (CAPS), Florida State University, Tallahassee, FL 32310 USA (e-mails: {leng, wliu, chung, dave}@caps.fsu.edu. Phone: 850-645-6944, fax: 850-645-1534).

Park's transformation where the three-phase voltage and current signals are transformed to the synchronously rotating frame. Under this method, the system is fairly stable as the controller mainly deals with dc quantities [12]. However, this method has phase dependent characteristic and it is suitable only for balanced three-phase systems.

Recently, a multiple adaptive feed-forward cancellation (MAFC) algorithm has been proposed in [13]. This algorithm does not need voltage information to extract harmonic current, which makes it invulnerable to contaminated voltages. In addition, this harmonic identification method is phase independent. That means it can identify harmonic contents in three-phases independently, even for unbalanced system or single-phase system.

Thus, the MAFC method is selected in the harmonic cancellation module. In this paper, the algorithm development is improved and the convergence of the harmonic detection process is rigorously guaranteed by verification of the persistent excitation condition.

Besides trying to cancel the harmonic currents, this paper also tries to compensate the reactive power consumed by the nonlinear load using the same active filter. By doing this, the power factor of the system can be improved and the capability of active filter can be fully used. To do that, reactive power drawn by nonlinear load is first calculated based on measured voltage and fundamental current estimated by the MAFC algorithm. Through Clarke transformations, the reactive power information is mapped to current control reference signal for compensation.

To aid the above-mentioned two functions and ensure the correct operation of active filter, an additional module is added to control voltage across the DC capacitor of the active filter. Similarly, the voltage control signal is finally transformed to current reference signal together with the harmonic cancellation and reactive power compensation signals. The three corrective signals are then summed up to form the reference signal for hysteresis current controller. Therefore, one active filter can compensate three-phase harmonic currents as well as reactive power in the power system, reducing the necessity to install extra reactive power compensator.

The rest of the paper is organized as follows. Section II explained the proposed control scheme in detail. Section III presents the simulation results under different operating conditions. Finally, conclusions are made in section IV.

II. CONTROL SCHEME

The proposed control scheme is illustrated in Fig. 2, which includes three modules: the harmonic cancellation module, the reactive power compensation module, and the DC capacitor voltage control module.

The harmonic cancellation module generates harmonic compensating signal and provides the fundamental current information to the reactive power compensation module. The reactive power compensation module calculates reactive power compensating signal. The DC capacitor voltage control module regulates the voltage across the DC capacitor. All compensating signals are summed up at the *abc*-frame to form the reference signal for the hysteresis current controller [12]. Finally, gating signals are generated for the IGBT based switching devices. From above introduction, we can see that the harmonic cancellation and the reactive power compensation modules are used towards the nonlinear load, while the DC voltage control module is used for the active power filter. This is the reason why the signs assigned to the three signals are '+', '+', and '-', respectively as shown in Fig. 2. The algorithms used in three control modules are introduced as follows.

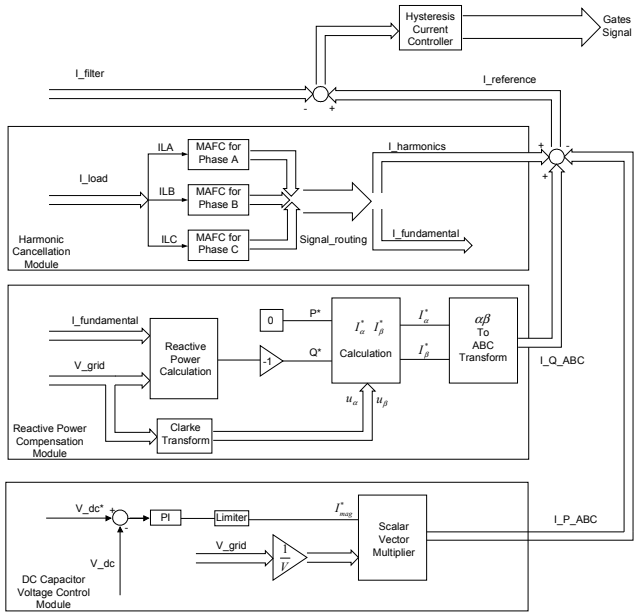

Fig. 2. Flow chart of the control scheme

A. MAFC Algorithm

Assuming the nonlinear load current *I_load* has the following form:

$$I\_load = I_{L1}\sin(\omega_1 t+\varphi_1)+I_{L3}\sin(\omega_3 t+\varphi_3) +.....+I_{Ln}\sin(\omega_n t+\varphi_n)+I_{dc} \quad (1)$$

where, the subscript n means the harmonic order, which are determined as $n = 2k+1$ (k = 0, 1, 2, …) and I_{Ln}, ω_n, φ_n and I_{dc} represent the amplitude, frequency and phase angle of the n_{th} harmonic component, and the dc component, respectively. Normally, due to delta connections in three-phase systems, the harmonic components with the order of $n = 3k$ (k = 1, 2, …) may not exist in the current waveform.

The first step of the adaptive law development is to parameterize equation (1). The phase φ_n and amplitude I_{Ln} are unknown and the current *I_load* is measured through a sensor with transfer function $W(s)$ to attenuate higher frequency noise. Then, we have the parameterized model as

$$z = W(s)\cdot I\_load = W(s)[I_{L1}\sin(\omega_1 t+\varphi_1)+I_{L3}\sin(\omega_3 t+\varphi_3) +.....+I_{Ln}\sin(\omega_n t+\varphi_n)+I_{dc}] \quad (2)$$

The load current can be rewritten as

$$I\_load = I_{L11}\sin\omega_1 t + I_{L12}\cos\omega_1 t + ... + I_{Ln1}\sin\omega_n t + I_{Ln2}\cos\omega_n t + I_{dc} \quad (3)$$

where

$$I_{L11} = I_{L1}\cos\varphi_1, I_{L12} = I_{L1}\sin\varphi_1, \ldots, I_{Ln1} = I_{Ln}\cos\varphi_n, I_{Ln2} = I_{Ln}\sin\varphi_n \quad (4)$$

The parametric model can be obtained as $z = W(s)\theta^{*T}\phi$ where z is the measurement, θ^* is the unknown vector and ϕ is the generated vector which are defined as

$\theta^* = [I_{L11}, I_{L12}, ..., I_{Ln1}, I_{Ln2}, I_{dc}]^T$ and

$\phi = [\sin\omega_1 t, \cos\omega_1 t, ..., \sin\omega_n t, \cos\omega_n t, 1]^T$.

Define θ and $\hat{z}$ as the estimate of θ^* and z respectively, where $\theta = [\hat{I}_{L11}, \hat{I}_{L12}, ..., \hat{I}_{Ln1}, \hat{I}_{Ln2}, \hat{I}_{dc}]^T$. Then, the estimate of the amplitude I_{Ln} and the phase angle φ_n of each harmonic component at time t can be calculated by

$$\hat{I}_{Ln}(t) = \sqrt{\hat{I}^2_{Ln1}(t) + \hat{I}^2_{Ln2}(t)}, \quad \hat{\varphi}_n(t) = \cos^{-1}\left(\frac{\hat{I}_{Ln1}(t)}{\hat{I}_{Ln}(t)}\right) \quad (5)$$

To derive the adaptive law to get the estimates, the SPR-Lyapunov method is applied here. The estimation error is calculated as

$$\varepsilon = z - \hat{z} = W(\theta - \theta^*)^T\phi = -W\tilde{\theta}^T\phi \quad (6)$$

where $\tilde{\theta} = \theta - \theta^*$. Now, we can define a state-space equation that has the input $-\tilde{\theta}^T\phi$ and the output ε as

$$\dot{e} = A_c e + B_c(-\tilde{\theta}^T\phi)$$
$$\varepsilon = C_c e \quad (7)$$

where A_c, B_c, and C_c are the matrices associated with a state space representation that has a transfer function $W(s) = C_c^T(sI - A_c)^{-1}B_c$.

Now, consider the Lyapunov-like function as

$$V(\tilde{\theta}, e) = \frac{e^T P_c e}{2} + \frac{\tilde{\theta}^T\Gamma^{-1}\tilde{\theta}}{2} \quad (8)$$

where the adaptive gain matrix $\Gamma = \Gamma^T > 0$ and a positive definite matrix $P_c = P_c^T > 0$. Because W is a low pass filter with strictly positive real (SPR) property, P_c satisfies the Meyer-Kalman-Yakubovich (MKY) Lemma such that

$$P_c A_c + A_c^T P_c = -qq^T - vL_c \quad \text{and} \quad P_c B_c = C_c \quad (9)$$

for some vector q, matrix $L_c = L_c^T > 0$ and v>0 Then, the time derivative $\dot{V}$ can be calculated as

$$\dot{V}(\tilde{\theta}, e) = -\frac{1}{2}e^T qq^T e - \frac{1}{2}ve^T L_c e - \varepsilon\tilde{\theta}^T\phi + \tilde{\theta}^T\Gamma^{-1}\dot{\tilde{\theta}} \quad (10)$$

The $\dot{V}$ becomes negative semi-definite ($\dot{V} \le 0$) if we choose the adaptive law as

$$\dot{\theta} = \dot{\tilde{\theta}} = \Gamma\varepsilon\phi \quad (11)$$

The adaptive gain matrix Γ can be chosen as a diagonal matrix such that $\Gamma = diag(\gamma)$ for some $\gamma > 0$. The individual harmonic estimation formulas can be obtained as

$$\dot{\hat{I}}_{L11} = \gamma_{11}\varepsilon\sin\omega_1 t, \quad \dot{\hat{I}}_{L12} = \gamma_{12}\varepsilon\cos\omega_1 t, \ldots..$$
$$\dot{\hat{I}}_{Ln1} = \gamma_{n1}\varepsilon\sin\omega_n t, \quad \dot{\hat{I}}_{Ln2} = \gamma_{n2}\varepsilon\cos\omega_n t, \quad \dot{\hat{I}}_{dc} = \gamma_{dc}\varepsilon \quad (12)$$

Since the average of the integration of the matrix $\phi(t)\phi^T(t)$ consists of the elements that are formulated as linear combination of sinusoidal functions as shown below:

To guarantee harmonic estimate θ converges to unknown θ^*, the integral of $\phi(t)\phi^T(t)$ should be bounded as

$$\alpha_0 I \le \frac{1}{T_o}\int_t^{t+T_o}\phi(\tau)\phi^T(\tau)d\tau \le \alpha_1 I, \quad \forall t \ge 0 \quad (13)$$

with a level of excitation $\alpha_0 > 0$ with some $\alpha_1, T_o > 0$.

The matrix $\phi(t)\phi^T(t)$ consists of eight types of sine and cosine functions and the integration results become linear combination of sine and cosine functions as list in Table I.

TABLE I
INTEGRATION OF ELEMENTS OF $\phi(t)\phi^T(t)$

Elements of $\phi(t)\phi^T(t)$	$\int\phi(t)\phi^T(t)dt$	$\frac{1}{T_o}\int_t^{t+T_o}\phi(\tau)\phi^T(\tau)d\tau$ for $T_o = \frac{2\pi}{\omega_1}$
$\sin n\omega_1 t$	$-\frac{\cos n\omega_1 t}{n\omega_1}$	0
$\cos n\omega_1 t$	$\frac{\sin n\omega_1 t}{n\omega_1}$	0
$\sin^2 n\omega_1 t$	$\frac{t}{2} - \frac{\sin 2n\omega_1 t}{4n\omega_1}$	$\frac{1}{2}$
$\cos^2 n\omega_1 t$	$\frac{t}{2} + \frac{\sin 2n\omega_1 t}{4n\omega_1}$	$\frac{1}{2}$
$\sin n\omega_1 t \cdot \cos n\omega_1 t$	$\frac{\sin^2 n\omega_1 t}{2n\omega_1}$	0
$\sin n\omega_1 t \cdot \cos m\omega_1 t$	$-\frac{\cos(n-m)\omega_1 t}{2(n-m)\omega_1} - \frac{\cos(n+m)\omega_1 t}{2(n+m)\omega_1}$	0
$\sin n\omega_1 t \cdot \sin m\omega_1 t$	$\frac{\sin(n-m)\omega_1 t}{2(n-m)\omega_1} - \frac{\sin(n+m)\omega_1 t}{2(n+m)\omega_1}$	0
$\cos n\omega_1 t \cdot \cos m\omega_1 t$	$\frac{\sin(n-m)\omega_1 t}{2(n-m)\omega_1} + \frac{\sin(n+m)\omega_1 t}{2(n+m)\omega_1}$	0

(*) n and m are integers and $n \ne m$

For $T_o = \frac{2\pi}{\omega_1}$, the diagonal terms of the average integration matrix in (13) become 0.5 with zero off-diagonal terms. Therefore, the persistence existence (PE) condition of (13) can be satisfied with $T_o = \frac{2\pi}{\omega_1}$, $0 < \alpha_0 < \frac{1}{2}$, and $\alpha_1 > \frac{1}{2}$. In addition, it is easy to verify that ϕ and $\dot{\phi}$ are bounded ($\in L_\infty$), thus the adaptive law of (11) guarantees that $\theta \to \theta^*$ exponentially fast [14].

In real power systems, the fundamental frequency ω_1 may be disturbed by operating condition change. Therefore, fundamental frequency should be identified and used to update the harmonic estimation algorithm. Instead of using

PLL for fundamental frequency tracking, an adaptive law [15] is used to track the fundamental frequency, as is shown below.

$$\dot{\hat{\omega}}_1 = -\alpha \cdot \varepsilon \cdot \left[\sum_{n=1}^{N} \left(n \cdot t \cdot \hat{I}_{Ln1} \cos n\omega t - n \cdot t \cdot \hat{I}_{Ln2} \sin n\omega t \right) \right] \quad (14)$$

where $\dot{\hat{\omega}}_1$ is the derivative of estimated fundamental frequency, α is adaptive gain, ε is estimation error.

According to the two adaptive laws (12) and (14), the MAFC method can be illustrated using Fig. 3. Since $W(s)$ has higher cut-off frequency than harmonic components to be eliminated, it can be assumed as a unity factor in each harmonic estimation path.

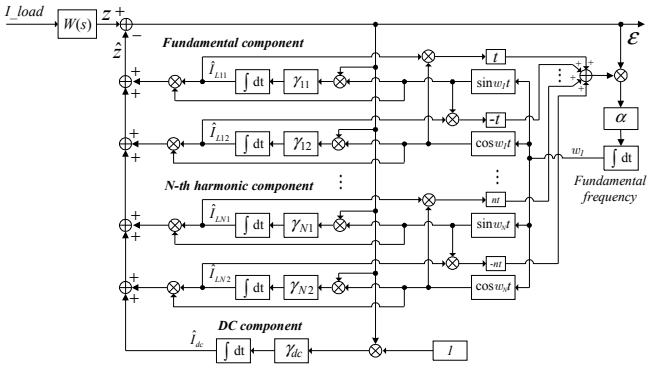

Fig. 3 Control block diagram of MAFC

B. Reactive Power Compensation

To compensate reactive power in the system, both voltage information and fundamental current information are needed. The former one is measured at PCC and the latter one can be estimated using the MAFC algorithm. In this paper, it is assumed that the voltage at PCC does not contain harmonics. Therefore, following equation can be used to calculate reactive power consumed by the nonlinear load [16]:

$$Q = \frac{1}{\sqrt{3}} \left[(u_a - u_b) i_c + (u_b - u_c) i_a + (u_c - u_a) i_b \right] \quad (15)$$

After calculating the reactive power, it is desired that the active filter inject $-Q$ reactive power to the PCC so as to compensate the reactive power consumed by the nonlinear load. Following equation is used to convert power-compensating signal to current compensating signal [16].

$$\begin{bmatrix} i_\alpha^* \\ i_\beta^* \end{bmatrix} = \frac{1}{\left(u_\alpha^2 + u_\beta^2\right)} \begin{bmatrix} u_\alpha & u_\beta \\ u_\beta & -u_\alpha \end{bmatrix} \begin{bmatrix} P^* \\ Q^* \end{bmatrix} \quad (16)$$

In (16), $\begin{bmatrix} P^* & Q^* \end{bmatrix}^T$ represents the desired output power for the reactive power compensation module, that is $P^* = 0, Q^* = -Q$, and $\begin{bmatrix} u_\alpha & u_\beta \end{bmatrix}^T$ is calculated using forward Clarke transformation as shown below.

$$\begin{bmatrix} u_\alpha \\ u_\beta \end{bmatrix} = \sqrt{\frac{2}{3}} \begin{bmatrix} 1 & -1/2 & -1/2 \\ 0 & \sqrt{3}/2 & -\sqrt{3}/2 \end{bmatrix} \begin{bmatrix} u_a \\ u_b \\ u_c \end{bmatrix} \quad (17)$$

Finally, reverse Clarke transformation is used to convert reactive power compensating signal from $\alpha\beta$ frame to abc frame according to (18).

$$\begin{bmatrix} i_{q\_a}^* \\ i_{q\_b}^* \\ i_{q\_c}^* \end{bmatrix} = \sqrt{\frac{2}{3}} \begin{bmatrix} 1 & 0 \\ -1/2 & \sqrt{3}/2 \\ -1/2 & -\sqrt{3}/2 \end{bmatrix} \begin{bmatrix} i_\alpha^* \\ i_\beta^* \end{bmatrix} \quad (18)$$

C. DC Capacitor Voltage Control

Since the voltage level across the DC capacitor is critical for the correct operation of active filters, a PI controller is used to regulate the DC voltage. As shown in Fig. 2, the output of the PI controller represents the magnitude of the corrective current reference signal. By assuming ideal switching devices, the power consumption for the DC voltage regulation has no reactive content. Thus, the generated corrective current reference signal should be in phase with the source voltage [17]. During implementation, the corrective current magnitude signal is multiplied with normalized three-phase source voltages to form the current reference signal for the DC capacitor voltage control module.

III. Simulation Results

To demonstrate the performance of the proposed control scheme, a power system shown in Fig. 4 is simulated in MATLAB/SIMULINK environment.

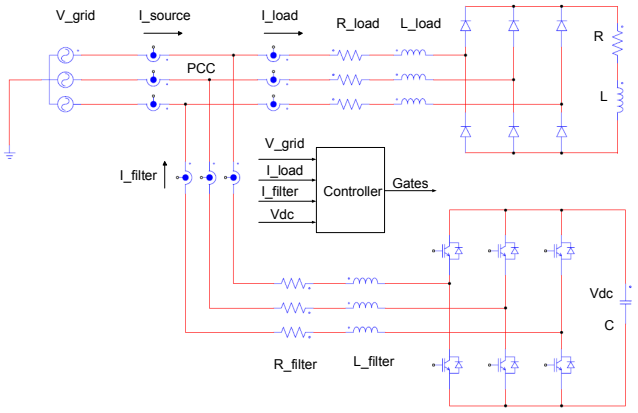

Fig. 4. Overview of the simulated system

The main electrical parameters of the simulated system shown in Fig. 4 are listed in Table II. The main control parameters of the simulated system are listed in Table III. The values in parenthesis represent the final values for step change tests.

TABLE II
MAIN ELECTRICAL PARAMETERS OF SIMULATED SYSTEM

Supply fundamental frequency	60 Hz (65Hz)
Supply voltages (Ph-Ph rms)	104 V
Diode rectifier load	R = 3 Ω (1.5 Ω), L = 0.5 mH
Active filter	C=1mF
Diode rectifier input impedance	R_load = 0.5 Ω, L_load = 0.1mH
Active filter output impedance	R_filter = 2mΩ, L_load = 2mH

TABLE III
MAIN CONTROL PARAMETERS OF SIMULATED SYSTEM

Sampling time	Ts = 0.01ms
Hysteresis band	Δi = 0.1A
MAFC gain	$\gamma_{n1} = \gamma_{n2} = 500, n = 1,5,7,11$ $\gamma_{n1} = \gamma_{n2} = 40, n = 13,17,19,23$ $\gamma_{dc} = 50$
Frequency estimation gain	$\alpha = 25$
PI controller	$K_p = 20, K_i = 1$
Limiter	$\Delta = \pm 1$

It should be noted that since the system is simulated under balanced operating condition, in most cases, only phase-A results are provided.

A. Harmonic Estimation

In this paper, only 1st, 5th, 7th, 11th, 13th, 17th, 19th, and 23rd order harmonic estimation are used for the MAFC algorithm. During harmonic estimation tests, the MAFC algorithm is tested in three operating conditions, i.e. harmonic estimation under fixed fundamental frequency, harmonic estimation under fundamental frequency change, and harmonic estimation under nonlinear load magnitude change.

Fig. 5 compares the measured and estimated load current in phase-A. The estimated load current is composed of the estimated dc offset, the fundamental component and the selected harmonic contents. It can be seen that the harmonic estimation algorithm can successfully identify the harmonic contents in the measurement.

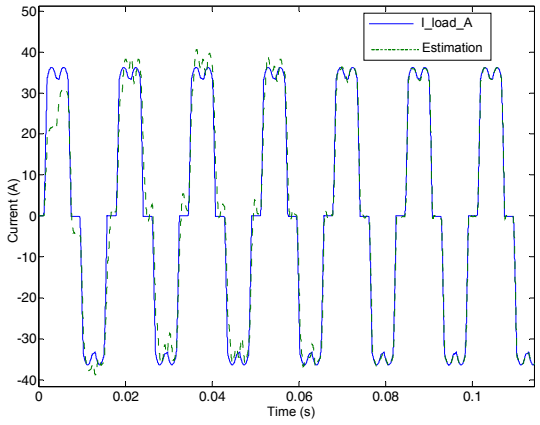

Fig. 5. Harmonic estimation under fixed fundamental frequency

Fig. 6 demonstrates the fundamental frequency tracking ability of the MAFC algorithm. For a fundamental frequency step change at 0.4, the estimation of fundamental frequency converges within 0.1 second. For the same test, the harmonic estimation results are provided in Fig. 7.

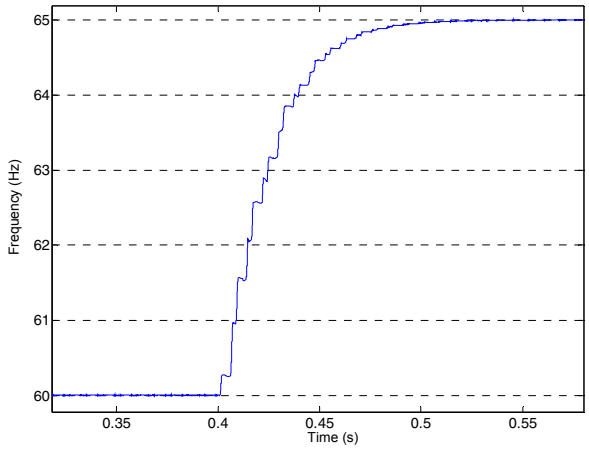

Fig. 6. Frequency response of MAFC

Fig. 7 shows phase-A harmonic estimation under fundamental frequency change. The fundamental frequency of the power system steps from 60 Hz to 65 Hz at 0.4 second.

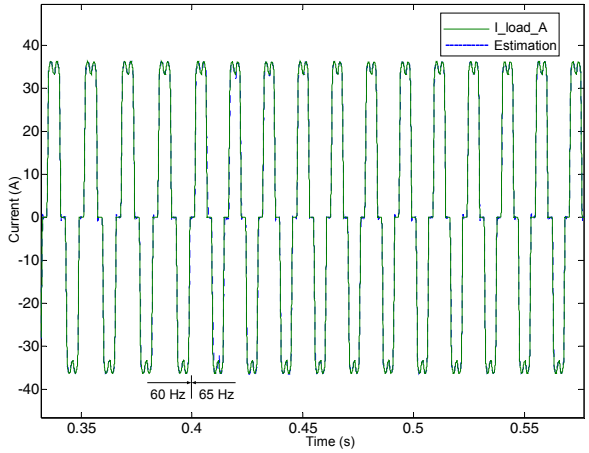

Fig. 7. Harmonic estimation under fundamental frequency change

Fig. 8 shows the harmonic estimation results under nonlinear load magnitude change. During this test, the fundamental frequency is fixed at 60Hz, while the resistance of diode rectifier load is decreased by half at 0.8 second. The MAFC algorithm adapts this dynamical change in approximately three cycles.

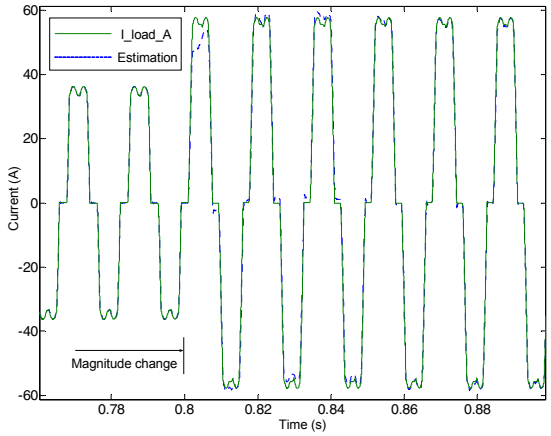

Fig. 8. Harmonic estimation under nonlinear load magnitude change

B. Harmonic Cancellation

After the performance of MAFC algorithm is verified, the closed-loop tests are conducted to study the harmonic cancellation performance. Similar to previous harmonic estimation tests, three tests are conducted, which are test under fixed fundamental frequency, test under fundamental frequency change, and test under nonlinear load magnitude change. Simulation results are provided in Figs. 9-13 accordingly.

Figs. 9 and 10 compare diode rectifier phase-A load current and source current after compensation under fixed fundamental frequency. Before harmonic cancellation module takes effect, the source current equals to the load current, which has observable waveform distortion. From Fig. 9, it can be seen that after harmonic cancellation, source current waveform distortion is significantly reduced and the source current approximates a sinusoidal waveform very well.

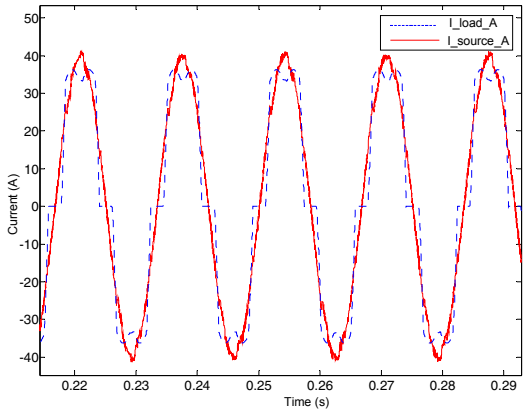

Fig. 9. Load current and source current

Fig. 10 is the spectrum analysis of the above two signals. It can be seen that the proposed control scheme can effectively suppress harmonic components and the total harmonic distortion (THD) is reduced from 24.12% to 2.37%.

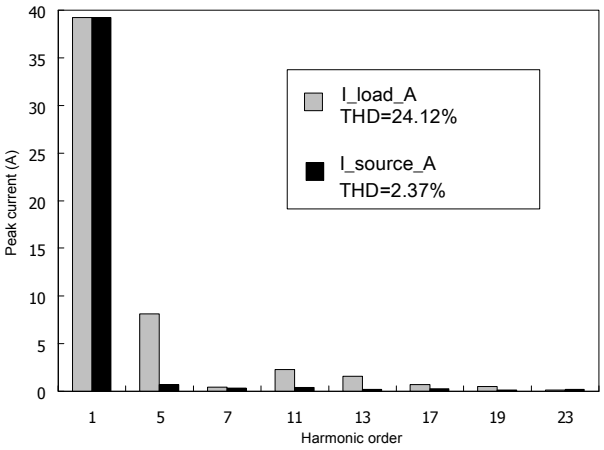

Fig. 10. Load current and source current spectrum analysis

Fig. 11 shows three-phase source currents after compensation under fixed fundamental frequency. It should be noted that harmonic cancellation is conducted at individual phase independently, so the algorithm can even be applied to unbalanced operating conditions.

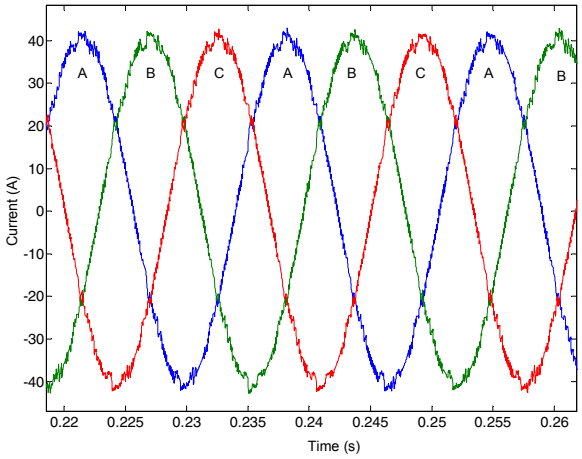

Fig. 11. Three-phase source currents after compensation

Fig. 12 shows the results of the fundamental frequency change test and compares the diode rectifier phase-A load current and the source current after compensation. For a fundamental frequency step change at 0.4 second (from 60 Hz to 65 Hz), the compensated source current can track the frequency change immediately.

Fig. 13 is the simulation result for nonlinear load magnitude change test. The resistance of diode rectifier load is decreased by half at 0.8 second. It can be seen that the harmonic cancellation scheme can provide good performance for this test as well.

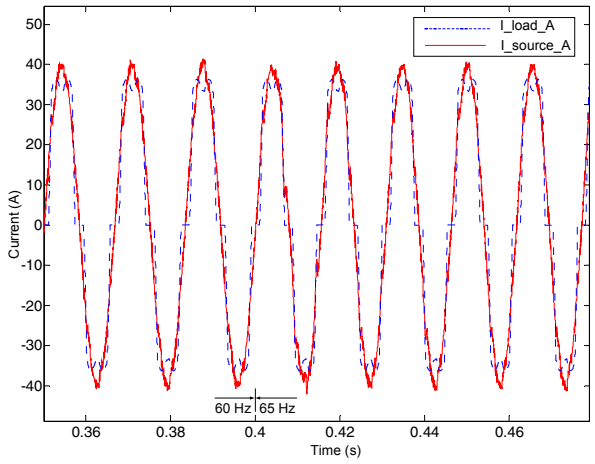

Fig. 12. Load and source current under fundamental frequency change

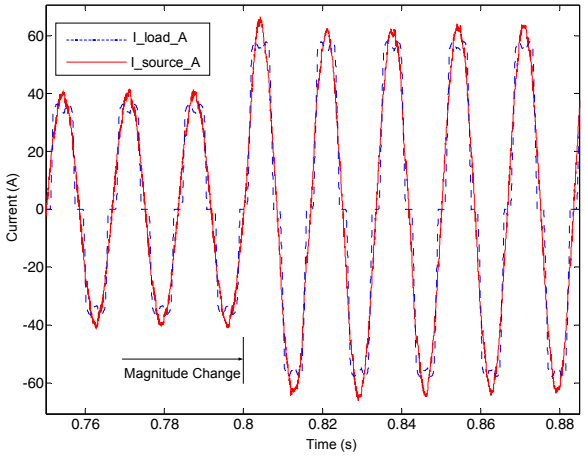

Fig. 13. Load and source current under nonlinear load magnitude change

C. Reactive Power Compensation

After harmonic cancellation module has been verified to work properly, reactive power compensation module is added to the active filter. Fig. 14 plots the phase-A voltage and current during reactive power compensation test. Before 1.2 second, although the source current has been compensated to nearly sinusoidal, a phase lag can be observed between the voltage and current, which indicates a power factor less than one at PCC. After 1.2 second, the reactive power compensation module takes effect and the voltage and current signal are in phase with each other, which indicates power factor improvement at PCC.

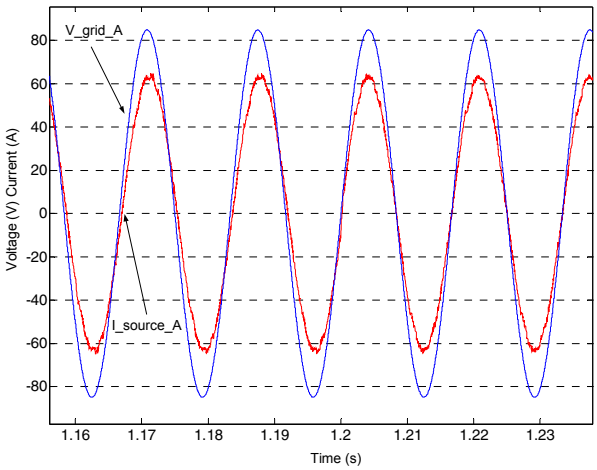

Fig. 14. Phase-A voltage and current during reactive power compensation

D. DC Capacitor Voltage Control

In this test, the DC capacitor voltage with and without control is compared, which demonstrates the effectiveness of the DC capacitor voltage control module.

Fig. 15 shows the DC capacitor voltage without control. It can be seen that DC voltage oscillates with frequency change, load magnitude change and reactive power compensation, which occurs at 0.4s, 0.8s and 1.2s, respectively.

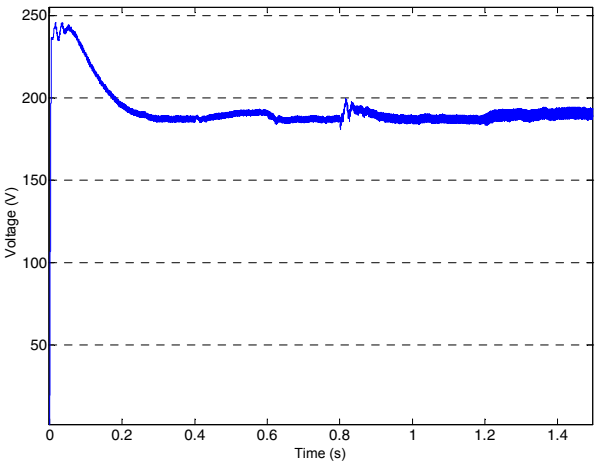

Fig. 15. DC capacitor voltage without control

Fig. 16 shows the DC capacitor voltage with control. The reference value is set at 200V. It can be observed that the DC voltage can be efficiently maintained at the desired value in spite of the same operating condition changes as Fig. 15.

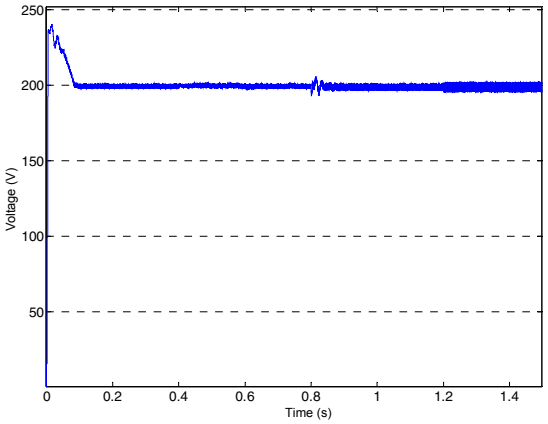

Fig. 16. DC capacitor voltage with control

E. Compensating Signals

To investigate the effect of the additional function modules (the reactive power compensation module, the DC capacitor voltage control module) on active filter, compensating signals as well as the final current reference signal for Phase-A are plotted in Fig. 17. It can be seen that adding additional function modules has increased the peak value of current reference signal, which in turn, increases the rating of the active filter.

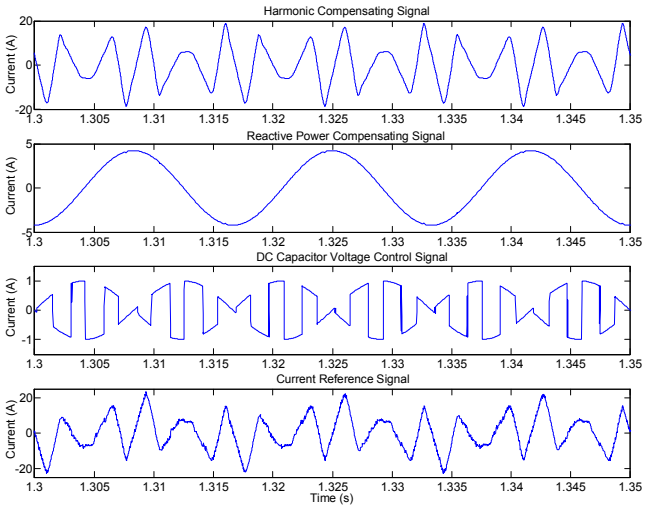

Fig. 17. Compensating signals and current reference signal for phase A

IV. CONCLUSIONS

A new control scheme is proposed to address harmonic current and reactive power problem in power systems. The proposed control scheme can compensate both harmonic current and reactive power in the system, which greatly improves power quality at the PCC. Compared with conventional control schemes, the proposed control scheme has the advantages of straight forward to understood and simple to implement. Simulation results show the proposed control scheme has good steady state and dynamical performance. In the future, it will be investigated how to find optimal control schemes for the cases where harmonic and reactive power compensation requirement exceeds the rating of active filter.

REFERENCES

[1] H. Akagi, "New trends in active filters for power conditioning," IEEE Transactions on Industrial Applications, vol. 32, issue. 6, pp.1312-1322, Nov-Dec. 1996.

[2] J.S. Thorp, A.G. Phadke, and K.J. Karimi, "Real-Time Voltage Phasor Measurements for Static-State Estimation", IEEE Trans. on Power Apparatus and Systems, vol. PAS-104, no.11, pp. 3099-3106, November 1985.

[3] G.T. Heydt, "A New Method for the Calculation of Sub-transmission and Distribution System Transients Based on the FFT", IEEE Trans. on Power Delivery, vol.4, no.3, pp.1869-1875, July 1989.

[4] J. Svensson, " Synchronization methods for grid- connected voltage source converter", IEE Proc.- Generation, Transmission and Distribution, vol. 148, issue 3, pp. 229 – 235, May 2001.

[5] M. Rastogi, N. Mohan and A.A. Edris, "Filtering of harmonic currents, damping of resonances in power systems with a hybrid active filter," in Proc. IEEE APEC'95 Conf., 1995, pp.607-612.

[6] H. Akagi, Y. Kanazawa, and A. Nabae, "Instantaneous reactive power compensators comprising switching devices without energy storage components", *IEEE Trans. on Industry Applications*, vol. IA-20, no.3, pp.625-630, May/June 1984.

[7] F. Z. Peng, and J. S. Lai, "Generalized instantaneous reactive power theory for three phase power systems," IEEE Transactions on Instrument and Measurement, vol. 45, pp. 293-297, Feb. 1996.

[8] H. L. Jou. "Performance comparison of the three-phase active-power-filler algorithms," IEE Proc.-Generation Transmission and Distribution. vol. 142, issue, 6, pp. 646 - 652, Nov. 1995.

[9] H. Fujita, and H. Akagi, "A practical approach to harmonic compensation in power systems-series connection of passive and active filters," IEEE Transactions on Industry Applications, vol. 27, issue. 6, pp. 1020-1025, Nov-Dec. 1991.

[10] F. Z. Peng, H. Akagi, and A. Nabea, "Compensation characteristics of the combined system of shunt passive and series active filters," IEEE Transactions on Industry Applications, vol. 29, issue. 1, pp. 114-152, Jan-Feb. 1993.

[11] P. Jintakosonwit, H. Fujita, H. Akagi, and S. Ogasawara, "Implementation and performance of cooperative control of shunt active filters for harmonic damping throughout a power distribution system," IEEE Transactions on Industry Applications, vol. 39, issue. 2, pp. 556-564, March-April 2003.

[12] N. Mariun, A. Alam, S. Mahmod, and H. Hizam, "Review of control strategies for power quality conditioner," in 2004 Proc Power and Energy Conf., pp. 109-115, Nov. 2004.

[13] L. Qian, D. Cartes, and Q. Zhang, "Three-Phase Harmonic Selective Active Filter Using Multiple Adaptive Feed Forward Cancellation Method," Power Electronics and Motion Control Conference, vol. 2, pp. 1-5, August 2006.

[14] Petros A. Ioannou, Jing Sun, *Robust Adaptive Control.* Prentice-Hall, 1996.

[15] S. Osowski, "Neural network for estimation of harmonic components in a power system," IEE Proc C.- Generation, Transmission and Distribution, vol. 139, Issue 2, pp. 129 – 135, March 1992.

[16] Hirofumi Akagi, Edson Hirokazu Watanabe, Mauricio Aredes *Instantaneous Power Theory and Applications to Power Conditioning.* Wiley IEEE Press, 2007.

[17] J. H. Xu, C. Lott, S. Saadate, and B, Davat, "Simulation and experimentation of a voltage source active filter compensating current harmonics and power factor," in 20th Conf. Industrial Electronics, Control and Instrumentation, 1994, vol. 1, pp. 411-415